Journal of Materials Chemistry A

PAPER

View Article Online
View Journal | View Issue

Cite this: J. Mater. Chem. A, 2018, 6, 24186

A novel approach for facilitating the targeted synthesis of silicoaluminophosphates†‡

Nana Yan,[ab] Lei Wang,[a] Xiaona Liu,[ab] Pengfei Wu,[ab] Tantan Sun,[ab] Shutao Xu,[a] Jingfeng Han,[a] Peng Guo,*[a] Peng Tian*[a] and Zhongmin Liu*[a]

Received 21st August 2018
Accepted 25th October 2018

DOI: 10.1039/c8ta08134d

rsc.li/materials-a

The targeted synthesis of crystalline microporous silicoaluminophosphate (SAPO) molecular sieves (MSs) with desired topologies is challenging. Conventionally, the trial-and-error approach assisted by computational methods is widely utilized for this exploration. The identification of predicted organic structure-directing agents (OSDAs) by this method is usually based on a neutral aluminophosphate or pure silica framework as the initial structural model, ignoring the host–guest interaction. To some extent, this may affect the prediction result. Herein, we present a novel approach called **RSS** (**R**efining, **S**ummarizing, and **S**earching), which is used for identifying appropriate OSDAs for synthesizing specific SAPO MSs. The **RSS** approach is mainly based on understanding the structural roles of the alkyl groups of OSDAs and the host–guest interaction elucidated from refinement analysis against experimental diffraction data. By adopting the **RSS** approach, the OSDAs of a small pore SAPO MS DNL-6 (**RHO** topology) have been extended from two types reported by us to fourteen additional commercialized ones. DNL-6 has shown promising CO_2/N_2 gas separation and the unique intermediate heptamethylbenezenium cations have been identified in DNL-6 during the methional-to-olefin (MTO) reaction in our previous work. The universality of this approach manifests the targeted synthesis of another SAPO MS SAPO-42 (**LTA** topology) by employing cheap commercialized OSDAs. Before our work, this material could only be synthesized using complex and expensive OSDAs in a toxic F^- medium.

Introduction

Silicoaluminophosphate (SAPO) molecular sieves (MSs), an analogue of conventional zeolites, are a class of crystalline microporous materials. Their basic building unit TO_4 (T = Al, Si, P, *etc.*) connects with its neighbours through corner sharing, generating a three-dimensional (3D) framework with well-defined cavities or channels of molecular sizes. Although there are 239 framework type codes (FTCs) approved by the International Zeolite Association-Structure Committee (IZA-SC), only a few SAPO forms, which can be used in acid catalysis, have been synthesized.[1] Based on the pore opening being delimited by the number of T atoms, they can be categorized as small pore (8 T), medium pore (10 T), large pore (12 T), and extra-large pore (>12 T) SAPO MSs, respectively. Among these SAPO materials, small pore SAPO MSs, especially SAPO-34 (FTC:**CHA**), have been extensively exploited in applications such as the methanol to olefin (MTO) process, the selective catalytic reduction (SCR) of nitrogen oxide species, gas separation, *etc.*[2,3] The commercialization of the MTO process in China has been accomplished by using the DMTO technology developed in our laboratory through the utilization of SAPO-34 based catalysts. Until now, there have been 23 units licensed and 12 are in operation in China, producing 6.46 million tons of olefins per year.[2]

Beside engineering applications, we have also been focusing on fundamental research such as the exploration of new catalysts for industrial applications. A novel small pore SAPO MS with the **RHO** topology (denoted as DNL-6, DNL stands for Dalian National Lab) was reported by our laboratory.[4–8] From the structural point of view, one *d8r* connects with two *lta* cages, while one *lta* cage links with six *d8r*s, creating a 3D channel system through 8-ring pore openings. It is worth noting that the intermediate heptamethylbenezenium cations were identified in the *lta* cage of DNL-6 under real MTO conversion conditions due to its strong Brønsted acidity and unique topology.[9] Moreover, it has also shown promising CO_2/N_2 gas separation.[6] Compared with the synthesis of SAPO-34 by utilizing various organic structure-directing agents (OSDAs),[10] investigations on the synthesis of DNL-6 are rare. Until now, only two types of OSDAs (diethylamine

[a]National Engineering Laboratory for Methanol to Olefins, Dalian National Laboratory for Clean Energy, Dalian Institute of Chemical Physics, Chinese Academy of Sciences, Dalian 116023, China. E-mail: pguo@dicp.ac.cn; tianpeng@dicp.ac.cn; zml@dicp.ac.cn

[b]University of Chinese Academy of Sciences, Beijing 100049, China

† This paper is dedicated to the 70th anniversary of the Dalian Institute of Chemical Physics, Chinese Academy of Sciences.

‡ Electronic supplementary information (ESI) available. CCDC 1846955, 1846956, 1847057, 1847060, 1847056, 1847059, 1847055, 1847061, 1847054, 1847068, 1847058, 1846953 and 1856120. For ESI and crystallographic data in CIF or other electronic format see DOI: 10.1039/c8ta08134d

and *N*,*N*′-dimethylethylenediamine) reported by us have been utilized for synthesizing DNL-6.[4–8,11] Therefore, this stimulated our efforts to synthesize DNL-6 with tunable Si contents by employing a variety of commercialized OSDAs.

Conventionally, the discovery of novel SAPO MSs (or zeolites) and the synthesis of them with specifically targeted known topologies are achieved through the trial-and-error experimentation. The targeted synthesis of them is the dream of zeolite scientists. Although their crystallization processes are still elusive, many endeavors have been devoted to this field. For instance, Lewis and co-workers put forward a methodology that computationally grows chemically feasible OSDAs through a "van der Waals overlap" function in a given zeolite framework.[12] Since the OSDAs grown by Lewis' approach may not be synthetically feasible, researchers at Rice University utilized the chemical molecules as starting fragments and then computationally grew them through well-established chemical reactions.[13] Appropriate OSDA candidates are identified through a scoring function (the interaction between a putative OSDA and the zeolite, termed the "stabilization energy"). Using OSDAs predicted by this updated method, zeolites with **AEI**, **RTH**, **SFW**, and **STW** FTCs have been successfully synthesized.[14–17] Moreover, with the aid of the molecular modelling approach, Turrina *et al.* have reported a series of novel small pore SAPO MSs belonging to the ABC-6 zeolite family by employing a retrosynthetic co-templating method.[18,19] In most cases, the neutral aluminophosphate or pure silica frameworks are selected as the initial structural models when these computational methods are utilized.[16,20] Therefore, the host–guest interaction, to some extent, is ignored. Moreover, assigning the locations of tetrahedral (T) heteroatoms (Si in the SAPO and Al in the conventional aluminosilicate zeolite) is also challenging in the computational process since it is closely associated with the experimental conditions.[21,22]

Herein, we propose an alternative approach called **RSS** (**R**efine, **S**ummarize, and **S**earch) to facilitate the targeted synthesis of specified zeolites or SAPO MSs of known topologies. The **RSS** approach is mainly based on analyzing and understanding the structural roles of alkyl groups in OSDAs and the host–guest interaction revealed by refinement analysis against experimental diffraction data. The small pore SAPO DNL-6 is chosen as an example to illustrate this method in detail. The **RSS** approach is composed of three parts: (1) **R**efine the known as-made samples against diffraction data, including single crystal X-ray diffraction (SCXRD), powder X-ray diffraction (PXRD), and electron diffraction (ED). In this step, the locations of OSDAs and the host (framework)–guest (OSDAs) interaction can be identified based on the refinement against the experimental diffraction data; (2) **S**ummarize the structural roles of OSDAs; (3) **S**earch for suitable OSDA candidates among commercialized organic amines with similar structural features. In order to manifest the universality of this approach, another SAPO MS SAPO-42 (FTC:**LTA**), which was obtained by employing expensive OSDAs of large size in a toxic F^- medium,[23,24] can be synthesized by the utilization of cheap commercialized OSDAs through the **RSS** approach.

Results and discussion

Rietveld refinement of two known DNL-6s

As mentioned before, DNL-6 can be synthesized by employing diethylamine (DEA) and *N*,*N*′-dimethylethylenediamine (DMEDA) as OSDAs (denoted as DNL-6-DEA and DNL-6-DMEDA). Following the **RSS** approach, firstly, both structural models of the as-made samples are refined against PXRD data since they crystallize with a size of a few micrometers, which is too small to be investigated by conventional in-house SCXRD. The aim of this step is to identify the locations of OSDAs and the host–guest interaction between the framework and the OSDAs.

The as-made DNL-6-DEA synthesized based on our previous recipe has a uniform crystal size of *ca.* 2 μm (Fig. S1‡).[4] Its unit cell composition deduced from XRF and TGA measurements is $|DEA_{8.1}(H^+)_{7.5}(H_2O)_{3.3}|[Al_{23.7}Si_{8.1}P_{16.2}O_{96}]$. Only 7.5 (less than 8.1) protonated OSDAs were required to balance the negatively charged framework, which suggests that the OSDAs trapped in DNL-6 are partially protonated. The presence of a broadband around 3200–3300 cm^{-1} in the Raman spectra (Fig. S2‡), which is assigned to the N–H stretching mode of neutral amines, proves this result. Rietveld refinement against PXRD data (collected on a high-resolution STOE STADI P ESSENTIAL diffractometer in the Debye–Scherrer mode) combined with the simulated annealing algorithms is utilized to locate the atomic coordinates of OSDAs and the host–guest interaction. We and other research groups have used this combined method not only to explore the locations of OSDAs in SAPO-34/44,[10] germanosilicates,[25,26] and a series of novel borosilicates,[27] but also probe Brønsted acidic sites confined in the 10-ring channels of the ferrierite (**FER**) zeolite.[28] We note that the idealized **RHO** framework with the space group of $Im\bar{3}m$ (no. 229) has only one T atom and two O atoms in the asymmetric unit. Due to the alternating distribution of Al and P, the space group of DNL-6 is reduced to *I*432 (No. 211). The initial atomic coordinates of Al, P, and two O atoms in the asymmetric unit were deduced from the idealized **RHO** framework deposited in the IZA database of the zeolite structure.[1] The difference electron density map as shown in Fig. 1a, indicating the initial locations of the OSDAs, was calculated from the experimental PXRD data and simulated one of the SAPO-form **RHO** framework (without OSDAs) (details in the ESI‡). Simulated annealing is then employed for determining the positions of the DEA OSDAs. The final refinement converged at $R_p = 0.0165$ and $R_{wp} = 0.0240$ (Fig. 1b and Table S1‡) and revealed that DEA stretches across the *d8r*s and *lta* cage, simultaneously generating the classical hydrogen bonding with the framework oxygen in the 8-rings (N1–H6⋯O2: 3.265 (17) Å) (Fig. 1c and d). Using identical approaches, the positions of DMEDA and the hydrogen bonding in the DNL-6-DMEDA (unit cell composition: $|DMEDA_{8.5}(H^+)_{9.3}\ (H_2O)_{10.6}|[Al_{19.9}Si_{17.5}P_{10.6}O_{96}]$) are determined, which are similar to the ones observed in the DNL-6-DEA (Fig. 3a, S7‡).

Summarize the common structural roles of OSDAs in the DNL-6s

It is of significance to note three main structural features of the OSDAs in the DNL-6s:

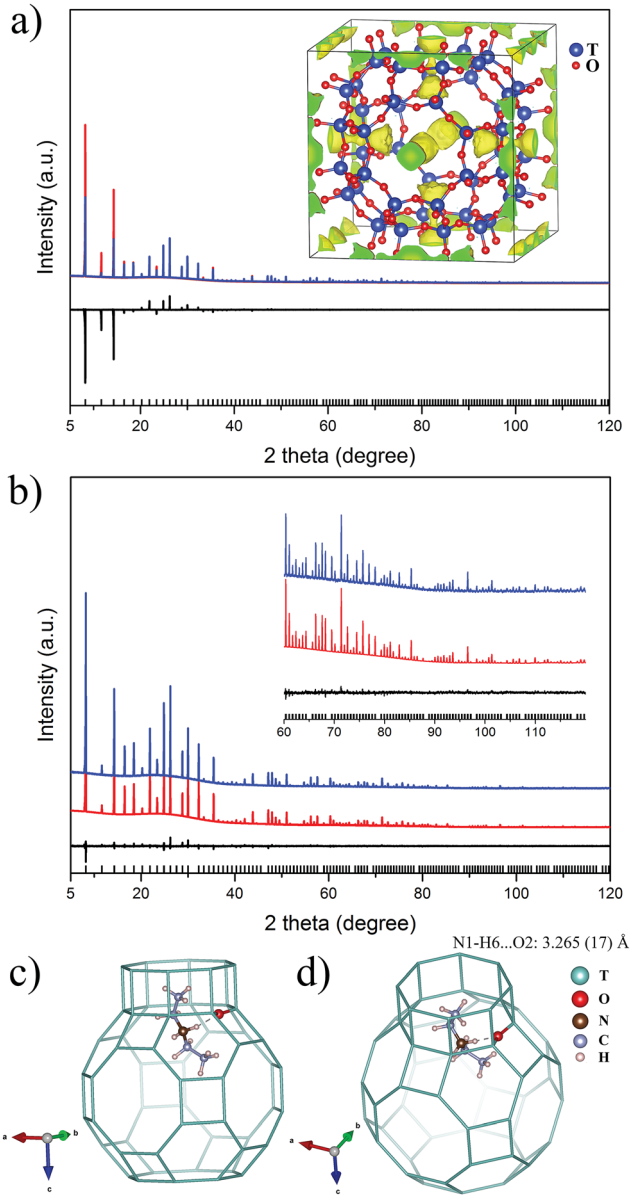

Fig. 1 (a) Plots for finding the DEA by applying the appropriate scale factor to the whole pattern. The inset shows the difference electron density map to locate positions of DEA through Rietveld refinement. (b) Final Rietveld refinement plots of DNL-6-DEA. The observed, calculated, and difference curves are in blue, red, and black, respectively. The vertical bars indicate the positions of Bragg peaks (Cu Kα1, λ = 1.5406 Å). The inset shows the high angle part of the profiles. (c) and (d) The location of DEA and the host–guest interaction in the as-made DNL-6-DEA sample from two perspectives, respectively. For clarity, the O atoms were omitted except for the one which makes the hydrogen bonding interaction with the N atom of DEA. The highly disordered water molecules have also been omitted for clarity.

(1) Classical hydrogen bonding between the OSDA and framework revealed by the final Rietveld refinement analysis is the key structural feature. In our previous work, the hydrogen bonding interactions have also been observed in SAPO-34/44 templated by *n*-butylamine and cyclohexylamine.[10] In most cases, these kinds of interactions are ignored in the computational modelling.

(2) One of the alkyl groups (ethyl group in DNL-6-DEA and methyl group in DNL-6-DMEDA) stretches into the *d8r*s.

(3) The other alkyl groups (ethyl group in DNL-6-DEA and *N*-methylethyleneamine in DNL-6-DMEDA) stabilize the *lta* cage. This observation is distinct from the previous strategy of stabilizing the *lta* cage, in which expensive OSDAs of large size were utilized.[23,24,29–32] This new finding can be extended to synthesizing other SAPO molecular sieves with *lta* cages.

Search for additional OSDAs and targeted synthesis of DNL-6s

The main task in this step is to search for new OSDAs among the commercialized organic amines that exhibit similar structural features to DEA and DMEDA. Thus, suitable organic amines should (1) form hydrogen bonds with the DNL-6 framework, preferably with oxygen in the 8-rings, and (2) have a longer alkyl group to stabilize the *lta* cage and a shorter one to stretch into *d8r*s (most likely the ethyl or methyl group). Taking the length of DEA and DMEDA into account, the backbone of suitable OSDA candidates might consist of five or six carbon atoms approximately, if the nitrogen atom is simply considered as carbon. Based on these predictions, several commercialized linear chain amines are identified and listed in Group I of Fig. 2, including *N*-methylethylamine (MEA), *N*-methylpropylamine (MPA), *N*-methylbutylamine (MBA), *N*-methylpentylamine (MPeA), *N*-ethylpropylamine (EPA), and *N*-ethylbutylamine (EBA). For quick verifications, our initial attempts are to synthesize DNL-6 using these linear secondary amines in Group I as OSDAs with a gel composition of 1.0 OSDA : 0.2 SiO_2 : 0.4 P_2O_5 : 0.5 Al_2O_3 : 50H_2O : 0.15 CTAB, which is the typical recipe for DNL-6-DEA.[4] In addition, a small amount (*ca.* 2–5 wt% relative to aluminum oxide) of the calcined DNL-6 seed with a crystal size of *ca.* 200 nm is added (details in the ESI‡). The PXRD results (Fig. S3a‡) indicate that these linear OSDAs can direct the synthesis of DNL-6, which is consistent with our predictions through the **RSS** approach.

Besides the linear OSDAs, commercialized branched secondary amines shown in Group II of Fig. 2 are also chosen for the targeted synthesis of DNL-6 using the same recipe mentioned above (details in the ESI‡). Preliminary PXRD results in Fig. S3b‡ illustrate that branched secondary amines can also be considered as effective OSDAs to direct the synthesis of DNL-6. The successful synthesis of DNL-6 by the utilization of linear and branched secondary amines stimulated our interest in the selection of cyclo-secondary amines with larger steric hindrance (Group III) and even primary amines (Group IV) as OSDAs to synthesize DNL-6. The tentative synthesis with the same recipe is conducted (details in the ESI‡). The PXRD results in Fig. S3c‡ indicate, to a certain extent, that both cyclo-secondary (Group III) amines and primary amines (Group IV) can direct the synthesis of DNL-6 as well.

Optimize synthesis conditions of DNL-6s templated by new OSDAs

Different amines (listed in Fig. 2) utilized as OSDAs in the tentative experiments could direct the synthesis of DNL-6; however, there are undesirable impurities such as SAPO-34,

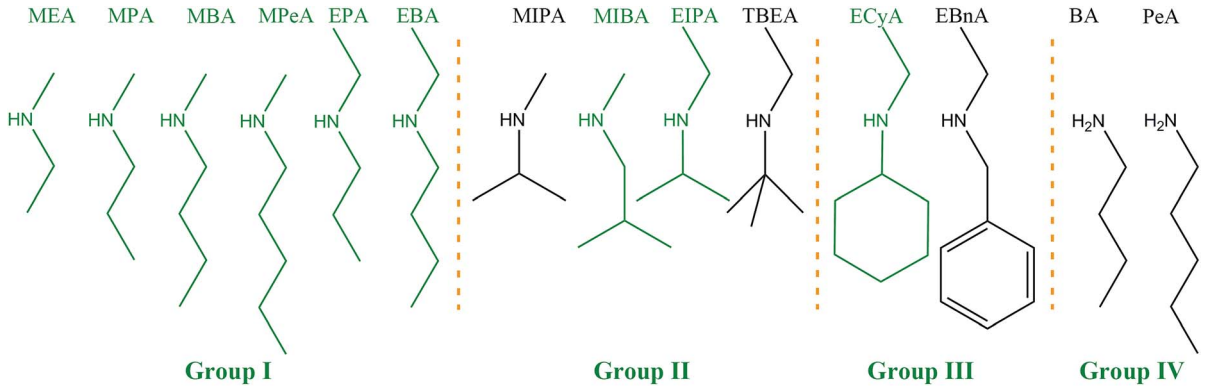

Fig. 2 The schematic representations of organic amine candidates. For clarity, the H atoms bonded to C atoms were omitted.

SAPO-42 (**LTA**) or amorphous phases. Therefore, a series of trials were performed by means of optimizing the gel composition, the silicon source, the aluminum source, and the amount of seed addition. Eventually, well-crystallized DNL-6s without any impurities using nine types of OSDAs (highlighted in green in Fig. 2) were obtained respectively. Representative optimized experimental parameters and results are shown in Table 1 and S2.‡ It is worth noting that by using optimized gel compositions (listed in Table 1) without any seed addition, DNL-6 can also be synthesized. However, some amorphous phases are still present when MPeA, EPA, and EBA are employed as OSDAs, and some SAPO-34 or/and SAPO-42 can be found in the products when MIBA, EIPA, and ECyA are used (Table S3‡). Consequently, nine DNL-6s obtained by using recipes listed in Table 1 are selected for further precise structural analysis.

SEM images (Fig. S4‡) of the as-made samples show that they have typical rhombic dodecahedral morphologies. ^{13}C MAS NMR spectra (Fig. S5a‡) confirm that OSDAs remain intact in the as-made DNL-6s. The unit cell compositions were also deduced from XRF and TGA (listed in Table 1). The OSDAs trapped in the nine DNL-6s are partially protonated since the number of OSDAs within one unit cell (deduced from XRF and TG) is more than the one of the protonated OSDAs of required. The appearance of the N–H stretching mode of neutral amines around 3200–3300 cm^{-1} in the Raman spectra (Fig. S2‡) also indicates that OSDAs in DNL-6 are partially protonated. Our previous work manifests that the dosage range of silicon for yielding pure DNL-6-DEA is small and the number of Si atoms per unit cell is nonadjustable when the DEA is employed as an OSDA in hydrothermal synthesis with CTAB as the surfactant.[4] Besides, by means of changing synthetic approaches[6,7] or utilizing different surfactants,[8] the Si content becomes adjustable by employing DEA as the OSDA. And high Si content DNL-6-DMEDA (about 11–17 per unit cell) can be obtained when DMEDA is utilized.[11] In this work, the Si content also plays an indispensable role in yielding the pure DNL-6. Moreover, the Si content can also be tuned from 7 to 12 per unit cell when different types of OSDAs are used as shown in Table 1. ^{29}Si MAS NMR of three samples (DNL-6-MBA, DNL-6-MPA, and DNL-6-EPA) with different Si contents has been performed to investigate the local atomic environment as shown in Fig. S5b, c, and d,‡ respectively. The strong peak at −91 ppm in the DNL-6-MBA with a low Si content suggests the presence of Si(OAl)$_4$ species in the framework. For the case of DNL-6-MPA with a medium Si content, a few Si(OSi) (OAl)$_3$ species at −95 ppm and Si(OAl)$_4$ species at −91 ppm are present. For DNL-6-EPA with a higher Si content, the ^{29}Si NMR spectrum is complex, and consists of five peaks (−91, −95, −100, −104, and −109 ppm) corresponding to Si(OSi)$_n$(OAl)$_{4-n}$ (n = 0–4) species, respectively.

Table 1 The gel compositions and unit cell compositions of DNL-6s templated by nine OSDAs highlighted in Fig. 2

Sample	OSDA (abbreviation)	Gel composition[a] OSDA : SiO_2 : P_2O_5 : Al_2O_3 : H_2O : CTAB (seed)	Unit cell compositions
DNL-6-MEA	*N*-Methylethylamine (MEA)	2 : 0.3 : 0.4 : 0.5 : 50 : 0.15 (20%)	$\|MEA_{9.2}(H^+)_{6.4}(H_2O)_{9.4}\|[Al_{22.6}Si_{9.2}P_{16.2}O_{96}]$
DNL-6-MPA	*N*-Methylpropylamine (MPA)	1.5 : 0.4 : 0.4 : 0.5 : 50 : 0.2 (20%)	$\|MPA_{8.0}(H^+)_{7.4}(H_2O)_{2.7}\|[Al_{22.6}Si_{10.2}P_{15.2}O_{96}]$
DNL-6-MBA	*N*-Methylbutylamine (MBA)	2 : 0.3 : 0.4 : 0.5 : 50 : 0.2 (20%)	$\|MBA_{7.1}(H^+)_{4.9}(H_2O)_{6.1}\|[Al_{22.9}Si_{7.1}P_{18.0}O_{96}]$
DNL-6-MPeA	*N*-Methylpentylamine (MPeA)	1.5 : 0.45 : 0.4 : 0.5 : 50 : 0.2 (40%)	$\|MPeA_{7.4}(H^+)_{6.3}(H_2O)_{5.0}\|[Al_{22.3}Si_{9.7}P_{16.0}O_{96}]$
DNL-6-EPA	*N*-Ethylpropylamine (EPA)	2 : 0.6 : 0.4 : 0.5 : 50 : 0.2 (40%)	$\|EPA_{7.3}(H^+)_{7.1}(H_2O)_{5.0}\|[Al_{21.4}Si_{12.3}P_{14.3}O_{96}]$
DNL-6-EBA	*N*-Ethylbutylamine (EBA)	1 : 0.55 : 0.4 : 0.5 : 50 : 0.2 (10%)	$\|EBA_{6.2}(H^+)_{5.6}(H_2O)_{2.7}\|[Al_{22.2}Si_{9.2}P_{16.6}O_{96}]$
DNL-6-MIBA	*N*-Methylisobutylamine (MIBA)	2.2 : 0.3 : 0.4 : 0.5 : 50 : 0.2 (40%)	$\|MIBA_{6.7}(H^+)_{6.9}(H_2O)_{5.0}\|[Al_{23.1}Si_{7.2}P_{16.2}O_{96}]$
DNL-6-EIPA	*N*-Ethylisopropylamine (EIPA)	2 : 0.45 : 0.4 : 0.5 : 50 : 0.2 (40%)	$\|EIPA_{7.4}(H^+)_{7.7}(H_2O)_{3.8}\|[Al_{22.4}Si_{10.9}P_{14.7}O_{96}]$
DNL-6-ECyA	*N*-Ethylcyclohexylamine (ECyA)	2 : 0.55 : 0.4 : 0.5 : 50 : 0.2 (40%)	$\|ECyA_{5.4}(H^+)_{5.1}(H_2O)_{4.5}\|[Al_{21.1}Si_{10.9}P_{16.0}O_{96}]$

[a] The amount of seed addition is based on the weight of Al_2O_3 in the synthesis system.

Rietveld refinement of DNL-6s templated by some OSDAs in Fig. 2

To investigate the locations of OSDAs and the host–guest interaction, these nine DNL-6s are analyzed by Rietveld refinement combined with simulated annealing. It turns out that all of the OSDAs as predicted stretch across *d8r*s and *lta* cages, leaving the shorter alkyl group (methyl or ethyl) and longer ones (linear, branched or cyclo-alkyl groups) in the *d8r*s and *lta* cages (Fig. 3b–j), respectively. More importantly, the hydrogen bonds between the OSDAs and framework are also identified (Fig. 3b–j) from the Rietveld refinement results (Table S1, Fig. S8–S16‡).

It is of interest to note that although there is no so-called "shorter" alkyl group in the primary amine BA molecule, it can still direct the synthesis of the DNL-6 with SAPO-34 as an impurity (Fig. S17a‡). Since the structural model of SAPO-34 templated by BA (denoted as SAPO-34-BA) has been elucidated in our previous work,[10] the Rietveld refinement of DNL-6-BA could be feasible by adding SAPO-34-BA as the second phase. Its difference electron density map (Fig. S17b‡) is different from the one observed in the DNL-6-DEA case. After running the simulated annealing algorithm, the isolated electron densities in the *d8r*s are interpreted as guest water molecules and the dangling ones are treated as BA molecules (Fig. S17c and d, and Table S1‡). In this case, the guest water molecules play a significant role in stabilizing the *d8r* building units, which was observed in our previous work regarding the aluminosilicate **RHO** zeolite family.[33] All these observations satisfy our criteria proposed in the second step of the **RSS** approach.

To further verify our **RSS** approach and have a deeper understanding of the structural roles of OSDAs, the secondary amines without longer alkyl groups (dimethylamine, DMA), the tertiary amine (triethylamine, TEA), and quaternary ammonium (tetraethylammonium, TEAOH) are also tested for synthesizing DNL-6 (details in the ESI‡). None of these OSDAs can be used for synthesizing DNL-6 as shown in Fig. S18,‡ even if the largest amount of seeds listed in Table 1 was added using the typical recipe of DNL-6-DEA. It can be attributed to the facts that (1) the longer alkyl group stabilizing the *lta* cage is absent in dimethylamine; (2) the protonated triethylamine molecule might be too big to form the hydrogen bond; (3) the hydrogen bonds between the TEA^+ and framework cannot be generated.

Targeted synthesis of SAPO-42 by the RSS approach

As mentioned above, the framework of DNL-6 is composed of *lta* cages linked *via d8r*s. The requirement that different alkyl groups of OSDAs stabilize distinct cages in size (*lta* cage and *d8r*) leads to the asymmetry of most OSDAs except for DEA. This inspires us to synthesize another small pore SAPO MS SAPO-42 (**LTA** topology), which is constructed using *lta* cages connected by the face-to-face mode through single 8-rings. It is highly possible that the symmetric OSDAs can direct the synthesis of SAPO-42.

Thus, dipropylamine (DPA) was selected as an OSDA for the tentative synthesis of SAPO-42. The initial trial (a gel composition of 1.7 DPA: 0.35 SiO_2: 0.4 P_2O_5: 0.5 Al_2O_3: 50H_2O: 0.15 CTAB in Fig. S19‡) indicates the successful synthesis of SAPO-42 in spite of some amorphous phases. Well-crystallized SAPO-42-DPA without any impurities was obtained by introducing SAPO-42 seeds (Table S6, S7, and Fig. S19‡). Then Rietveld refinement and simulated annealing are applied to analyze the location of DPA and the host–guest interaction of SAPO-42-DPA (step 1 of **RSS**). The symmetrical distribution of electron density on both sides of 8-rings reveals the location of DPA (Fig. 4a). And the final refinement manifests DPA stretches across the single 8-rings stabilizing two *lta* cages and the N atom is stuck in the 8-rings generates the classical hydrogen bonding with the

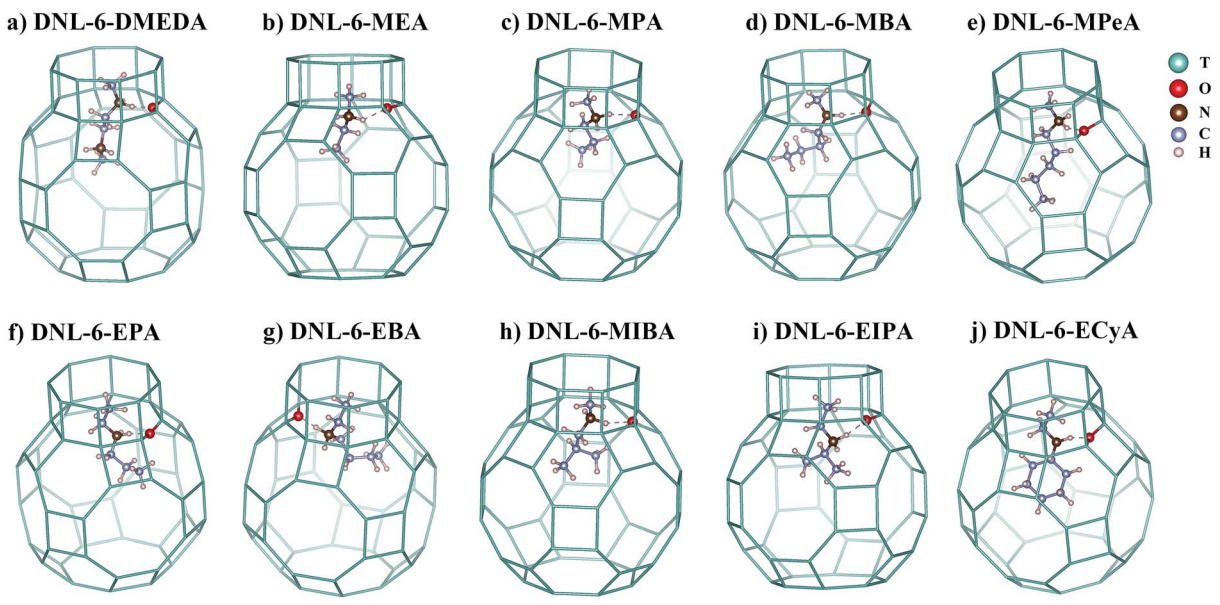

Fig. 3 (a–j) The locations of OSDAs and host–guest interactions in the DNL-6s templated by ten types of OSDAs.

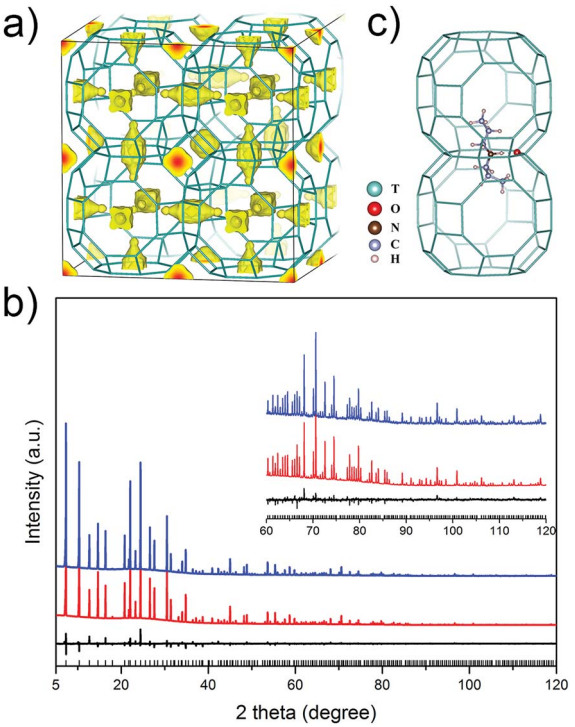

Fig. 4 (a) The difference electron density map indicates the initial locations of DPA and H_2O. (b) Final Rietveld refinement plots of SAPO-42-DPA. The observed, calculated, and difference curves are in blue, red, and black, respectively. The vertical bars indicate the positions of Bragg peaks (Cu Kα1, $\lambda = 1.5406$ Å). The inset shows the high angle part of the profiles. The PXRD data were collected in a 0.2 mm capillary. (c) The location of DPA and the host–guest interaction in SAPO-42-DPA. The unit cell composition of SAPO-42-DPA is $|DPA_{32.1}(H^+)_{17.9}(H_2O)_{24.3}|[Al_{88.8}Si_{32.3}P_{70.9}O_{384}]$.

framework oxygen (N1–H1⋯O1: 2.693 Å) (Fig. 4b, c, and Table S8‡) (step 2 of **RSS**). Then, amines with similar symmetrical structural features such as diethylamine (DEA) and dibutylamine (DBA) were identified as OSDAs to synthesize SAPO-42 (step 3 of **RSS**). The synthesis trails and corresponding results (Table S6 and Fig. S19‡) testify that, to some degree, both DEA and DBA have abilities to direct the synthesis of SAPO-42. Before our research, most SAPO-42 could only be synthesized by using complex and expensive OSDAs in a toxic F^- medium.[23,24]

Conclusions

In conclusion, a novel approach called **RSS** inspired by Rietveld refinement analysis is proposed to facilitate the targeted synthesis of SAPO **RHO**-type DNL-6 and **LTA**-type SAPO-42. It is anticipated that the **RSS** approach can be further employed to achieve the rational synthesis of other MSs or zeolites with designed structures and tailored properties.

Experimental

Materials synthesis

All synthesis experiments (details in the ESI‡) were carried out by the conventional hydrothermal method. Phosphoric acid, amines, and deionized water were mixed and then vigorously stirred. And then tetraethyl orthosilicate (TEOS) and aluminum isopropoxide were added sequentially. After stirring overnight, hexadecyl trimethyl ammonium bromide (CTAB) and a certain amount of seeds were added to the homogeneous gel. Then the thoroughly mixed gel was transported into a 35 ml Teflon-lined autoclave and crystallized at 200 °C with the rotation speed of 75 rpm. The final products were recovered by centrifugation, washed with distilled water repeatedly, and dried at 120 °C overnight.

Characterization

The PXRD data for the phase identification were collected on a PANalytical X'Pert PRO X-ray diffractometer with CuKα radiation ($\lambda = 1.5418$ Å) in Bragg–Brentano geometry. PXRD data for Rietveld refinement were collected on the STOE STADI P ESSENTIAL X-ray diffractometer equipped with a Mythen II detector in the Debye–Scherrer mode with pure Cu Kα1 radiation ($\lambda = 1.5406$ Å) (capillary: 0.2 or 0.3 mm, angle range: 5–120°, step size: 0.015°, total counting time: 16.5 h, room temperature). Scanning electron microscopy (SEM) was performed on a Hitachi SU8020 microscope with an accelerating voltage of 2 kV and a working distance of 6 mm. The elemental analysis for Si, Al, and P was conducted using a Philips Magix-601 X-ray fluorescence spectrometer (XRF). Thermogravimetric analysis (TGA) was performed on a TA Q-600 analyzer or a NETZSCH STA449F3 instrument at a heating rate of 10 °C min^{-1}. Raman spectra were obtained on a self-built system with a spectral resolution of 4 cm^{-1}. The laser line at 244 nm was used as an excitation source. The power of the laser line used for measuring at the samples was approximately 0.2 mW. The spectra of all samples were recorded at room temperature. The solid-state NMR experiments were recorded on a Bruker Avance III 600 spectrometer equipped with a 14.1 T wide-bore magnet using a 4 mm WVT double resonance MAS probe. The resonance frequencies of ^1H, ^{13}C and ^{29}Si are 600.13, 150.9 and 119.2 MHz, respectively. ^{13}C MAS NMR spectra were recorded using a cross polarization (CP, $^1H \rightarrow {}^{13}C$) sequence with a contact time of 4 ms and a recycle delay of 2 s at a spinning rate of 12 kHz. 400 scans were accumulated to achieve a satisfactory signal-to-noise ratio. The chemical shifts were referenced to adamantane with the upfield methine peak at 29.5 ppm. ^{29}Si MAS NMR spectra were recorded with a spinning rate of 8 kHz using high-power proton decoupling. 1000 scans were accumulated with a 10 s recycle delay. Chemical shifts were referenced to 4,4-dimethyl-4-silapentane sulfonate sodium salt at 0 ppm.

Rietveld refinement and simulated annealing

The approach for finding the initial positions of organic structure directing agents (OSDAs) was based on the method developed by Smeets and McCusker by using the program TOPAS 5.0.[27] Once the primary coordinates of Al and P and two O atoms in the asymmetric unit and space group are deduced as stated in the main text, the profile fitting started with cubic unit cell parameters of the **RHO** topology from the IZA database using

TOPAS 5.0. And then the optimized framework was obtained through geometrical refinement against the angle and distance restraints by the "only _ penalty" command. Since guest species such as structure-directing agents (SDAs) in the cavities have negligible influence on the high angle PXRD data, PXRD data at 2θ: 60°–120° were chosen to find the optimal scale factor between experimental PXRD data and simulated PXRD data of the optimized framework. Then the obtained scale factor was applied to the whole pattern, and therefore, the calculated electron difference density map can be generated, indicating the initial locations of guest species in the cavities. Simulated annealing was introduced to TOPAS 5.0 for determining appropriate locations of OSDAs. Moreover, since alkyl chains of amines are flexible, dihedral angles of its backbone are also optimized in the process of simulated annealing. After several runs of the simulated annealing algorithm, the initial positions could be located by fixing the unit cell parameters, atomic coordinates, peak shape parameters, and the scale factor. The final Rietveld refinement can be done by refining the aforementioned parameters. The final Rietveld refinement results are summarized in Table S1.‡

An identical approach was applied to the SAPO-42 material for finding the OSDA and the host–guest interaction. The final Rietveld refinement results are summarized in Table S8.‡

Conflicts of interest

There are no conflicts to declare.

Acknowledgements

Dr Peng Tian acknowledges financial support from the National Natural Science Foundation of China (No. 21676262) and Key Research Program of Frontier Sciences, Chinese Academy of Sciences (Grant No. QYZDBSSW-JSC040). Dr Peng Guo acknowledges financial support from the CAS Pioneer Hundred Talents Program (Y706071202). Dr Lei Wang acknowledges the China Postdoctoral Science Foundation (2018M630308) and DICP Outstanding Postdoctoral Foundation (2017YB07). We thank the kind help from Ms Wenna Zhang and Ms Lingyun Li for the theoretical calculation and solid-state NMR measurements, respectively.

Notes and references

1 http://www.iza-structure.org/databases/, Database of Zeolite Structures.
2 P. Tian, Y. Wei, M. Ye and Z. Liu, *ACS Catal.*, 2015, **5**, 1922–1938.
3 J. Xue, X. Wang, G. Qi, J. Wang, M. Shen and W. Li, *J. Catal.*, 2013, **297**, 56–64.
4 X. Su, P. Tian, J. Li, Y. Zhang, S. Meng, Y. He, D. Fan and Z. Liu, *Microporous Mesoporous Mater.*, 2011, **144**, 113–119.
5 P. Tian, X. Su, Y. Wang, Q. Xia, Y. Zhang, D. Fan, S. Meng and Z. Liu, *Chem. Mater.*, 2011, **23**, 1406–1413.
6 X. Su, P. Tian, D. Fan, Q. Xia, Y. Yang, S. Xu, L. Zhang, Y. Zhang, D. Wang and Z. Liu, *ChemSusChem*, 2013, **6**, 911–918.
7 D. Fan, P. Tian, S. Xu, Q. Xia, X. Su, L. Zhang, Y. Zhang, Y. He and Z. Liu, *J. Mater. Chem.*, 2012, **22**, 6568–6574.
8 M. Yang, P. Tian, L. Liu, C. Wang, S. Xu, Y. He and Z. Liu, *CrystEngComm*, 2015, **17**, 8555–8561.
9 J. Li, Y. Wei, J. Chen, P. Tian, X. Su, S. Xu, Y. Qi, Q. Wang, Y. Zhou, Y. He and Z. Liu, *J. Am. Chem. Soc.*, 2012, **134**, 836–839.
10 N. Yan, H. Xu, W. Zhang, T. Sun, P. Guo, P. Tian and Z. Liu, *Microporous Mesoporous Mater.*, 2018, **264**, 55–59.
11 P. Wu, M. Yang, W. Zhang, S. Zeng, M. Gao, S. Xu, P. Tian and Z. Liu, *Chin. J. Catal.*, 2018, **39**, 1511–1519.
12 D. W. Lewis, D. J. Willock, C. R. A. Catlow, J. M. Thomas and G. J. Hutchings, *Nature*, 1996, **382**, 604.
13 R. Pophale, F. Daeyaert and M. W. Deem, *J. Mater. Chem. A*, 2013, **1**, 6750–6760.
14 J. E. Schmidt, M. W. Deem, C. Lew and T. M. Davis, *Top. Catal.*, 2015, **58**, 410–415.
15 J. E. Schmidt, M. A. Deimund, D. Xie and M. E. Davis, *Chem. Mater.*, 2015, **27**, 3756–3762.
16 T. M. Davis, A. T. Liu, C. M. Lew, D. Xie, A. I. Benin, S. Elomari, S. I. Zones and M. W. Deem, *Chem. Mater.*, 2016, **28**, 708–711.
17 J. E. Schmidt, M. W. Deem and M. E. Davis, *Angew. Chem., Int. Ed.*, 2014, **53**, 8372–8374.
18 A. Turrina, R. Garcia, P. A. Cox, J. L. Casci and P. A. Wright, *Chem. Mater.*, 2016, **28**, 4998–5012.
19 A. Turrina, R. Garcia, A. E. Watts, H. F. Greer, J. Bradley, W. Zhou, P. A. Cox, M. D. Shannon, A. Mayoral, J. L. Casci and P. A. Wright, *Chem. Mater.*, 2017, **29**, 2180–2190.
20 A. W. Burton, G. S. Lee and S. I. Zones, *Microporous Mesoporous Mater.*, 2006, **90**, 129–144.
21 A. B. Pinar, C. Márquez-Álvarez, M. Grande-Casas and J. Pérez-Pariente, *J. Catal.*, 2009, **263**, 258–265.
22 J. Dědeček, Z. Sobalík and B. Wichterlová, *Catal. Rev.*, 2012, **54**, 135–223.
23 R. Martínez-Franco, Á. Cantín, A. Vidal-Moya, M. Moliner and A. Corma, *Chem. Mater.*, 2015, **27**, 2981–2989.
24 J. E. Schmidt, S. I. Zones, D. Xie and M. E. Davis, *Microporous Mesoporous Mater.*, 2014, **200**, 132–139.
25 S. Smeets, L. Koch, N. Mascello, J. Sesseg, L. B. McCusker, M. Hernández-Rodríguez, S. Mitchell and J. Pérez-Ramírez, *CrystEngComm*, 2015, **17**, 4865–4870.
26 L. Xu, L. Zhang, J. Li, K. Muraoka, F. Peng, H. Xu, C. Lin, Z. Gao, J.-G. Jiang, W. Chaikittisilp, J. Sun, T. Okubo and P. Wu, *Chem.–Eur. J.*, 2018, **24**, 9247–9253.
27 S. Smeets, L. B. McCusker, C. Baerlocher, S. Elomari, D. Xie and S. I. Zones, *J. Am. Chem. Soc.*, 2016, **138**, 7099–7106.
28 L. Wang, H. Xu, N. Yan, S. Correll, S. Xu, P. Guo, P. Tian and Z. Liu, *CrystEngComm*, 2018, **20**, 699–702.
29 M. Castro, R. Garcia, S. J. Warrender, A. M. Z. Slawin, P. A. Wright, P. A. Cox, A. Fecant, C. Mellot-Draznieks and N. Bats, *Chem. Commun.*, 2007, 3470–3472.

30 A. Corma, F. Rey, J. Rius, M. J. Sabater and S. Valencia, *Nature*, 2004, **431**, 287–290.
31 F. J. Elie, B. Nicolas, E. A. Kirschhock Christine, B. Rebours, A. A. Quoineaud and A. Martens Johan, *Angew. Chem., Int. Ed.*, 2010, **49**, 4585–4588.
32 L. Schreyeck, J. Stumbe, P. Caullet, J.-C. Mougenel and B. Marler, *Microporous Mesoporous Mater.*, 1998, **22**, 87–106.
33 P. Guo, J. Shin, A. G. Greenaway, J. G. Min, J. Su, H. J. Choi, L. Liu, P. A. Cox, S. B. Hong, P. A. Wright and X. Zou, *Nature*, 2015, **524**, 74–78.